Development of an Automated Knee Rehabilitation Device*

Lucas Handalián[1], Enrique D. Ferreira[1], Eduardo G. Hernandez-Martinez[2], Mario Ramírez-Neria[2]

***Abstract*— This paper presents an automated knee rehabilitation system designed to assist patients during the gait cycle. The system utilizes a predictive model based on a neural network to generate trajectories of the knee motion from data captured by a motion capture system. Also, some control schemes, a PID, a Second Order Sliding Mode Control, and an Active Disturbance Rejection Control, were implemented to follow these trajectories, considering knee dynamics and external disturbances. Finally, the experimental setup was developed to implement and compare these controllers. This adaptable solution has potential applications for post-surgical patients, athletes, and children with motor difficulties.**

I. INTRODUCTION

Knee rehabilitation is a critical process aimed at restoring joint function, reducing stiffness, and improving overall range of motion. The rehabilitation therapies could include the use of different electromechanical or robotic devices inside or outside medical centers [21]. The challenge for these devices is to follow the gait cycles depending of velocities of walking, intensity of the steps and the rythm and shapes of the cycle that could be different for each person.

Examples of robotics-based knee rehabilitation are given in [15], [10] and [4]. The common sensor for the measurement of the gait cycle are inertial measurement units (IMU's) [2] or infrared capture systems like in [6]. A simple robotic systems is the design of a knee brace controlled by a DC motor following the procedure of a Knee Ankle Foot Orthosis (KAFO). It is desirable for the knee brace to be portable, light and personalised for every patient. Some of the most important commercial companies in these solutions are Ottobock®[15] and Hocoma®[10]. The actual main disadvantage of the available products are the high costs for the most of patients, in the most of countries and their medical services. Also, the algorithms for the robotics setup are in continuous improvement due the complexity of the trajectories and the non-modeled perturbations appeared in real gait cycles [21].

The control strategies for the case of robotics-based knee rehabilitation are emerging by the robotics community [11], [3]. The focus of controllers canceling non-modeled disturbances have not been addressed, in the best of our knowledge.

*This work was supported by the Agencia Nacional de Investigación e Innovación de Uruguay (ANII).

[1]Lucas Handalián and Enrique D. Ferreira are with the Engineering Department, Universidad Católica del Uruguay, Montevideo, Uruguay lucasg.handalian@ucu.edu.uy, enrique.ferreira@ucu.edu.uy

[2]Eduardo G. Hernandez-Martinez and Mario Ramirez-Neria are with the Institute of Applied Research and Technology, Universidad Iberoamericana Ciudad de México, México eduardo.gamaliel@ibero.mx, mario.ramirez@ibero.mx

This paper presents the development of a controlled knee brace designed to assist patients during the swing phase of the gait cycle, offering an adaptable alternative for knee joint rehabilitation. The system aims to generate and track accurate knee trajectories, with potential applications in post-surgical rehabilitation, athletic training, and motor assistance for children with gait disorders.

The main contributions of this work are summarized in the following points.

- A knee brace is designed using a personalized manufacturing process for every patient. It is driven by a DC servomotor with a *STM32F407* microcontroller.
- A predictive model of the gait is developed training a Long Short-Term Memory (LSTM) neural network from data gathered using a Vicon motion capture system®[12]. This allows the generation of personalized gait trajectories adapted to each patient's walking pattern.
- Three control strategies to track the predicted trajectories were implemented and compared; a Proportional-Integral-Derivative (PID) controller, a second order Sliding Mode Controller (SMC) and an Active Disturbance Rejection Control (ADRC) strategy.

The paper is organized as follows. Section II describes the knee brace manufacturing process. The section III presents the design of the predictive model for the trajectories of the knee. The controllers are described in section IV. The experimental results and discussion are given in Section V. Finally, some conclusion remarks and future work are given in Section VI.

II. KNEE BRACE DESIGN

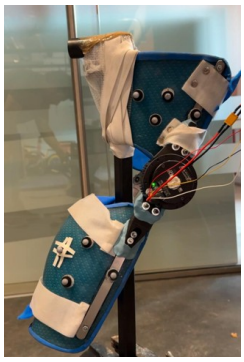

Fig. 1: Knee brace prototype

A custom mold of the subject's limb is created with the guidance of an orthotist, commonly used for lower limb

orthoses to ensure comfort. The RMD-x6 motor from My Actuator®[19], generating $5Nm$ of torque, was chosen for its suitability and high-speed communication. A 3D-printed coupling connects the motor to the system. The design of a knee brace involves the application of a plaster bandage to the limb, the creation of a mold, and the use of thermoplastic material for the formation. After shaping, the knee brace axes are aligned and EVA foam is added for comfort. This process results in a custom orthosis, as shown in Figure 1.

The control architecture of the knee brace is shown in the Figure 2. The automated rehabilitation system uses a *STM32F407* development board by STMicroelectronics® [18], running real-time control algorithms. It was developed in *Simulink*® [14] with the *Waijung 18*® [1] library, which generates embedded code directly from *Simulink*® models.

The system architecture shown in Figure 2 involves several interconnected modules that link the hardware with the predictive model and the control algorithms.

1) *Data Acquisition and Processing on PC.* The gait data capture process is performed using Vicon Nexus® cameras which record the motion of reflective markers placed on the device in real time. The collected data is then processed in Matlab®[13], where the knee joint angle is computed. This angle is used as input to an LSTM neural network, which predicts future joint angles.
2) *Serial Communication with Embedded Board.* The predicted angles from the LSTM model are transmitted to the embedded system via serial communication, and the reference trajectory is updated at 100 Hz to ensure smooth tracking.
3) *Control Execution on Embedded System.* The control algorithm (PID, SMC, or ADRC) runs on the embedded system at 1000 Hz, transmitting the control signal to the motor via RS485. The control signal is used as a reference to an internal PI controller that generates the actual action applied to the motor. The motor then applies torque to minimize trajectory deviations, while real-time knee angle feedback is sent back to the system, allowing for dynamic adjustments throughout the gait cycle.

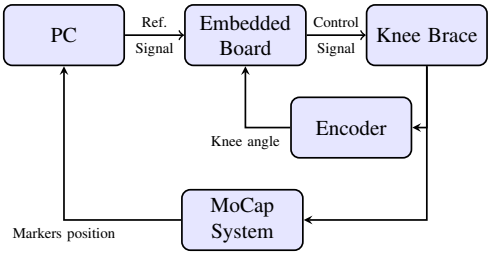

Fig. 2: System architecture

III. GAIT TRAJECTORIES

A. Capture of motion data

For the estimation of knee angles, dynamic gait data was collected using a Vicon® motion capture system. Reflective markers were strategically placed on the orthosis, including on the external and internal axes of the joint and along the brace segments, ensuring tracking of its movement with sub-millimeter precision (see Figure 3a). Marker trajectories were processed to reconstruct the knee brace's motion and predict future joint angles using machine learning techniques.

Data collection was performed at 100Hz over three days, capturing more than 2500 steps at different walking speeds on a treadmill. This dataset, cleaned and filtered to remove noise, formed the basis for building predictive models of knee angle behavior.

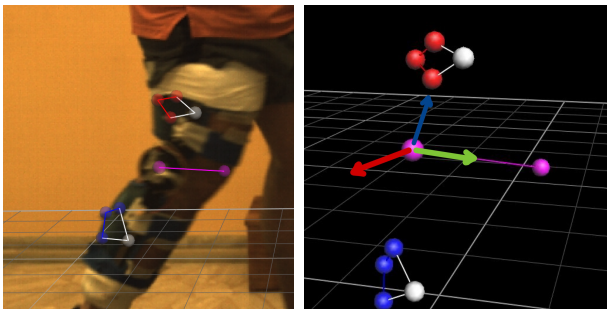

(a) Markers Superimposed on a Video Footage

(b) red: *X-axis*, green: *Y-axis*, blue: *Z-axis*

Fig. 3: Knee brace axes and markers superimposed on video footage during gait trials.

To compute the knee angles, the marker data was transformed into a local reference system fixed to the knee orthosis (see Figure 3b). This system consisted of:

- *Y-axis (Sagittal)*: Aligned with the axis between the condyles, representing flexion and extension.
- *X-axis (Frontal)*: Perpendicular to the Y-axis and an auxiliary axis along the knee brace.
- *Z-axis (Transverse)*: Perpendicular to both X and Y axes, forming an orthogonal system.

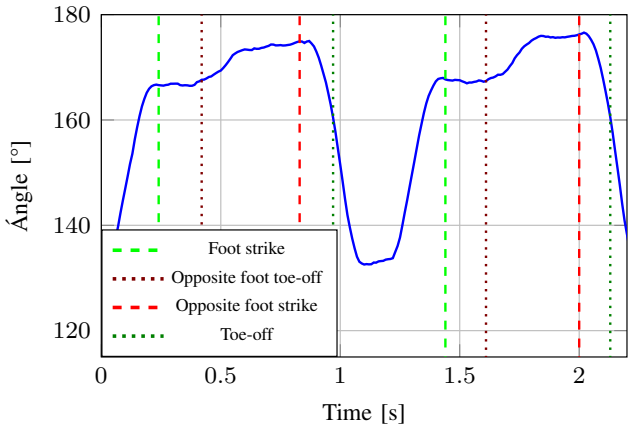

Fig. 4: Right knee angle during the gait cycle.

The flexion-extension angle was calculated in the plane defined by the X and Z axes, using the vectors formed between specific markers (see Figure 4).

This knee brace-relative reference system minimized external influences (e.g., slight motion capture shifts) and ensured consistent angle calculation across different trials and conditions.

B. Neural Network training

A neural network architecture was developed to predict future knee joint angles to be used as a reference signal for real-time control in robotic knee rehabilitation systems. It follows a *sequence-to-sequence* modeling approach, where the input consists of the 50 most recent knee joint angles, and the output corresponds to the predicted knee angles for the next 10 time steps, providing an adjustable control horizon.

To capture temporal dependencies in human gait dynamics, the architecture uses LSTM-based layers, ideal for modeling long-range temporal correlations [8]. These layers are interspersed with *dropout layers* to reduce over-fitting by randomly deactivating neurons during training, enhancing generalization [5]. Multiple LSTM depth and hidden unit configurations were tested to identify the optimal network topology, as shown in Table I.

The networks were trained using the *Adam* optimizer, known for its adaptive learning rate and robustness against non-stationary gradients. A *custom loss function* was developed to emphasize the biomechanical relevance of different gait phases, ensuring that errors are weighted according to clinical significance. Prediction errors during the *swing phase*, when the knee experiences rapid angular changes and the motor actively assists, receive a higher penalty, focusing the network on accurately predicting this dynamically critical phase. Conversely, errors during the *stance phase*, when the knee remains stable and the motor is inactive, are weighted less and excluded from both *mean squared error* (MSE) and *mean absolute error* (MAE) calculations. Thus, the cost function was defined as:

$$\text{Loss} = \begin{cases} (y_{\text{true}} - y_{\text{pred}})^2, & \text{if } y_{\text{true}} \leq \text{MAX} \\ (y_{\text{true}} - y_{\text{pred}})^2 \times \text{Weight}, & \text{if } y_{\text{true}} > \text{MAX} \end{cases}$$

where:

- y_{true}: Knee angle.
- y_{pred}: Predicted knee angle.
- MAX: Knee angle threshold (165°) that marks the transition to the *stance phase*.
- Weight: Penalty reduction factor in the *stance phase*, set to 0.05.

Note for the swing and stance phases:

- Swing Phase ($y_{\text{true}} \leq$ MAX). In this phase, the motor assists the knee movement, requiring accurate predictions. Errors are penalized quadratically with $(y_{\text{true}} - y_{\text{pred}})^2$ to emphasize the need for precise trajectory forecasting.
- Stance Phase ($y_{\text{true}} >$ MAX). During the stance phase, the motor is inactive, and prediction errors are less critical. Quadratic errors are downweighted by the *Weight* factor, reducing their contribution to the overall loss.

Finally, the training protocol utilized *sliding window sequences* extracted from continuous knee angle time series during treadmill-assisted walking trials. Each training sample included a fixed-length input window (50 time steps) and a target window (10 time steps).

To prevent overfitting and improve generalization, *early stopping* was used to monitor *validation loss*, reverting to weights with the lowest validation error. Validation sequences, from gait cycles not in the training set, were used to assess the model's generalization. The dataset was split into 70% for training, 15% for validation, and 15% for testing.

IV. CONTROL STRATEGIES

The trajectory tracking system receives the predicted knee joint angle (named as the reference signal $r(t)$) from the trajectory generator as input and calculates the actuator current required to follow the desired trajectory $u(t)$. The trajectory generator updates its predictions at a frequency of 100 Hz, while the feedback signal $y(t)$ from the motor encoder is sampled at 1 kHz.

Three control schemes were implemented: Proportional-Integral-Derivative (PID), Second Order Sliding Mode Control (SMC), and Active Disturbance Rejection Control (ADRC). Each controller was designed considering the operational requirements of the system.

All controllers apply a filter to the reference signal $r(t)$ using the following transfer function:

$$H_{ref}(s) = \frac{1 + Ts}{1 + \alpha s}$$

where $T = 0.04$ and $\alpha = 0.08$.

Additionally, whenever a derivative term is used, it is computed using a filtered derivative:

$$H_D(s) = \frac{\alpha s}{s + \alpha}$$

with $\alpha = 100$.

A saturation limit of ± 5A was applied to the control signal to prevent excessive currents. To account for static friction in the actuator, a dead-zone compensation term of $0.2 \cdot \text{sign}(u(t))$ was also included.

The following subsections describe the formulation and implementation of each control strategy.

A. Proportional-Integral-Derivative Controller

The PID control signal is computed as:

$$\begin{aligned} u(t) = {} & K_p \left(B \cdot r(t) - y(t) \right) \\ & + \int \left[K_i \left(r(t) - y(t) \right) + w_\alpha \left(-u + u_{sat} \right) \right] dt \\ & + K_d \frac{d \left(C \cdot r(t) - y(t) \right)}{dt} \end{aligned}$$

where:

- $r(t)$ is the reference signal.
- $y(t)$ is the knee angle given by the encoder.
- $u(t)$ is the current signal of the DC motor as the control input.
- K_p, K_i, K_d: Proportional, integral and derivative gains.

- B, C: Factors to reduce the impact of rapid reference changes.
- w_α: Antiwindup factor. Limits the integral contribution when the actuator reaches saturation.

Tuning and parameter selection: The controller was tuned experimentally as follows:

$$K_p = 0.35 \quad K_i = 2.5 \quad K_d = 0.003$$
$$B = 0.85 \quad C = 0.25 \quad w_\alpha = 20$$

B. Second Order Sliding Mode Control

A second order sliding mode control [17] [20] was implemented to achieve robust and accurate trajectory tracking for the knee brace system, which is subject to disturbances. The following outlines the implementation steps.

1) Sliding Surface Definition: The sliding surface $\sigma(t) = 0$ is designed to guide the system towards the desired behavior:

$$\sigma(t) = \dot{e}(t) + K_p e(t) \tag{1}$$

where $e(t) = r(t) - y(t)$ is the tracking error, $\dot{e}(t)$ is its derivative and K_p is the gain defining the convergence rate of the error.

2) Control Law: The control law drives the system towards the sliding surface and keeps $e(t)$ close to 0, as long as the model uncertainties and disturbances are bounded [16].

$$u(t) = \frac{1}{b}\left(-K_d\frac{dy(t)}{dt} + \alpha\sqrt{|\sigma(t)|}\,\mathrm{sgn}(\sigma(t)) + \beta\int \mathrm{sgn}(\sigma(t))\,dt\right),$$

where $\sigma(t)$ is the sliding variable, b is the control gain, K_d is the derivative gain, α and β are gains for the switching and integral terms, respectively.

3) Parameter Tuning: The controller was tuned experimentally as follows:

- $K_p = 10$ for fast error convergence.
- $K_d = 0.005$ for damping to avoid oscillations.
- $\alpha = 750$ to balance robustness and reduction in chatter.
- $\beta = 1250$ for low-frequency disturbance rejection.
- $b = 7900$ as the control gain.

C. Active Disturbance Rejection Control (ADRC)

ADRC is a control technique designed for systems with uncertain dynamics and external disturbances. It uses an *Extended State Observer* (ESO) to estimate the states and disturbances of the system, which are then compensated [7] [9].

First, it is assumed that the Knee system can be modeled by:

$$\ddot{y} = f(x(t)) + bu(t) + d(t) \tag{2}$$

where $y(t)$ is the output, $f(x)$ represents uncertain system dynamics, b is the control gain, u is the control action, and $d(t)$ is the external disturbance. The tracking error is defined as:

$$e(t) = y(t) - r(t), \tag{3}$$

where $r(t)$ is the reference trajectory. Thus, system (2) transforms into:

$$\ddot{e}(t) = bu(t) + P_t(t), \tag{4}$$

where the total disturbance P_t, is given by:

$$P_t(t) = f(x) + d(t) - \ddot{r}$$

The system (4) is reformulated into an augmented state-space representation, as follows

$$\mathbf{x} = \begin{bmatrix} x_1 \\ x_2 \\ x_3 \end{bmatrix} = \begin{bmatrix} e(t) \\ \dot{e}(t) \\ P_t(t) \end{bmatrix}, \quad \dot{\mathbf{x}} = \begin{bmatrix} x_2 \\ bu + x_3 \\ 0 \end{bmatrix}$$

where x_3 represents the total disturbance P_t. We assume that the disturbance varies slowly to consider $\dot{x}_3 = 0$ in the nominal system. The ESO estimates the system states and disturbance, with the observer dynamics given by:

$$\dot{\hat{x}}_1 = \hat{x}_2 + \lambda_1(x_1 - \hat{x}_1)$$
$$\dot{\hat{x}}_2 = bu + \hat{x}_3 + \lambda_2(x_1 - \hat{x}_1)$$
$$\dot{\hat{x}}_3 = \lambda_3(x_1 - \hat{x}_1),$$

where $\lambda_1, \lambda_2, \lambda_3$ are the observer gains. These are tuned to ensure fast convergence of the estimates to the actual states and disturbances. The control law is defined as:

$$u(t) = -\frac{1}{b}\left(K_p e + K_d\hat{x}_2 + \hat{x}_3\right)$$

where K_p and K_d are the proportional and derivative gains, respectively.

The observer gains are computed to have its poles satisfy the following polynomial:

$$(s^2 + 2\omega_o s + \omega_o^2)(s + \omega_o) = 0$$

The resulting observer gains are then:

$$\lambda_1 = 3\omega_o, \quad \lambda_2 = 3\omega_o^2, \quad \lambda_3 = \omega_o^3$$

For the controller, the desired closed-loop dynamics are defined by:

$$(s^2 + 2\zeta_c\omega_c s + \omega_c^2) = 0$$

where ω_c is the controller natural frequency and ζ_c is the damping ratio. The control gains are:

$$K_p = \omega_c^2, \quad K_d = 2\zeta_c\omega_c$$

The observer frequency is chosen such that:

$$\omega_o \geq 3\omega_c$$

which ensures the observer reacts faster than the controller, allowing the controller to use accurate estimates.

The parameters used in the implemented system are:

- Observer frequency: $\omega_o = 140$
- Controller frequency: $\omega_c = 12$
- Damping factor: $\zeta_c = 0.95$
- System gain: $b = 7900$
- Proportional gain: $K_p = 144$
- Derivative gain: $K_d = 22.8$

V. RESULTS AND DISCUSSION

A. Neural Network Performance

The selection of the neural network for the prediction of knee joint angle was based on a trade-off between model complexity and predictive performance, quantified using both *Mean Squared Error* (MSE) and *Mean Absolute Error* (MAE) (Table I). This approach aimed to mitigate overfitting risks while maximizing predictive accuracy.

TABLE I: LSTM network characteristics and performance (MAE and MSE).

Network	LSTM Layers	Model Size (param)	MAE	MSE
1	1	4.682	1.02	1.64
2	1	17.546	1.03	1.79
3	1	67.850	0.61	0.62
4	1	266.762	0.52	0.43
5	2	29.642	1.76	4.91
6	2	87.498	2.89	11.13
7	2	116.618	0.88	1.34
8	3	21.322	1.72	4.69
9	4	70.986	2.51	8.39
10	8	63.482	2.99	13.46
11	3	8.522	1.36	3.16
12	3	38.154	1.62	3.92

Among the evaluated architectures, Network 1 has one of the lowest MSE (1.64) despite its relatively smaller model size. This result highlights the model's generalization capability compared to alternative configurations. Furthermore, its MAE further supports its predictive performance (Table I).

Figure 5 illustrates the knee angle predictions generated by Network 1. The model successfully captures the temporal dynamics of knee motion, showing high correspondence with observed data, particularly during the *swing phase, shown as interest zone*, where the assistive system is designed to provide active support.

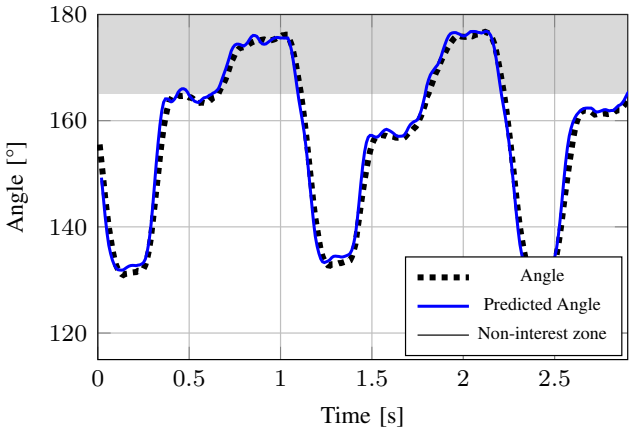

Fig. 5: Fifth step ahead prediction for Model 1.

These findings underscore the need to balance model complexity and predictive performance. Although larger architectures typically introduce computational overhead, the results indicate that Network 1 achieves acceptable accuracy while maintaining reasonable computational efficiency. Consequently, Network 1 is identified as the most suitable model for real-time knee angle prediction in this rehabilitation application.

B. Control System Validation

The performance of PID, SMC, and ADRC controllers was assessed based on MSE, MAE, IAE, control signal smoothness, and undershoot.

1) Tracking Error Metrics: Key metrics used to evaluate performance during the swing phase include:

- **MSE:** Measures average squared error.
- **MAE:** Evaluates average error magnitude.
- **IAE:** Cumulative absolute error over time.
- **Undershoot:** Percentage drop in output after disturbance or transients.

Control Signal Smoothness: Smooth control is crucial to prevent discomfort and mechanical wear.

Validation Procedure: Pre-recorded gait trajectories were used to test the controllers while the knee orthosis was suspended vertically.

TABLE II: Comparison of key performance metrics across control strategies.

Control	MSE ($^{\circ 2}$)	MAE (°)	IAE (°)	Undershoot (%)
PI-D	103,63	8,03	33.433,64	4,41
SMC	88,27	7,52	31.395,54	2,99
ADRC	179,27	11,17	46.567,68	7,67

Validation Results: The SMC controller outperformed others in tracking accuracy, achieving the lowest MSE, MAE, and IAE values. The ADRC showed higher errors, while PID had intermediate performance. For **undershoot**, all controllers maintained low values, with SMC performing the best.

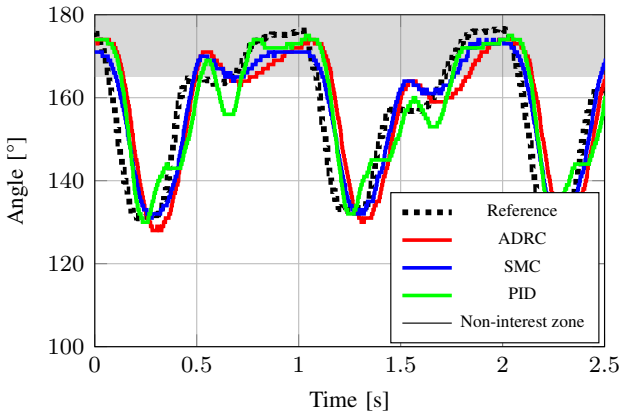

Fig. 6: Reference tracking performance for the three controllers implemented.

In terms of control signals, PID was the smoothest and SMC had more abrupt changes, while ADRC presented small oscillations.

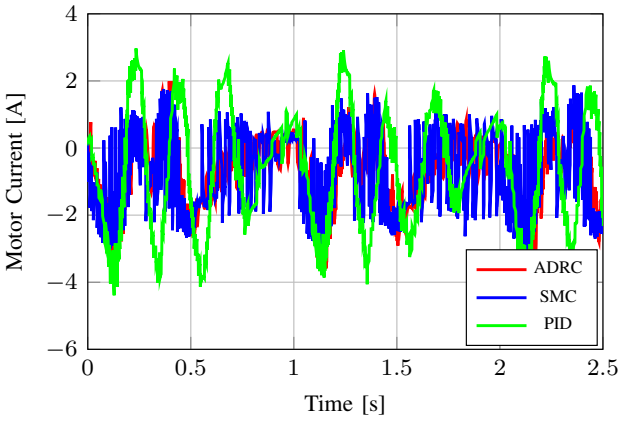

Fig. 7: Control signal results for the implemented controllers.

In summary, SMC offers the best balance of tracking, stability, and control quality, making it the most suitable for knee orthosis systems. ADRC could improve with better tuning.

VI. CONCLUSION AND FUTURE WORK

The knee orthosis prototype met the main objectives, successfully generating and following knee joint trajectories using an integrated control system for a specific user. The LSTM-based trajectory generator predicted knee angles smoothly and consistently, making it adaptable to individual gait patterns.

The control strategies (PID, SMC, ADRC) were evaluated, with PID performing reliably in simple scenarios, SMC offering effective tracking in dynamic conditions, and ADRC showing potential for disturbance rejection, although this could not be fully validated. Future testing under real gait conditions is necessary

The comparative analysis highlighted the trade-offs between simplicity and robustness, suggesting potential for real-world rehabilitation applications. The system's flexibility positions it as a promising tool for personalized rehabilitation.

Several future directions are proposed to enhance and validate the system under more realistic and challenging conditions:

- *Real-world validation:* Test controllers in real gait scenarios with disturbances.
- *Clinical trials:* Assess the system's impact on rehabilitation with real patients.
- *System robustness:* Improve resilience to noisy inputs and atypical gait.
- *Additional sensors:* Integrate advanced sensors (e.g., EMG, IMUs) to enhance data quality.
- *User interface:* Develop a clinician-friendly interface for real-time adjustments.
- *Biomechanical impact:* Analyze energy consumption and muscle activation.
- *Expanded applications:* Adapt for athletes in recovery and children with motor disabilities.

ACKNOWLEDGMENT

We would like to sincerely thank the Uruguayan National Agency for Research and Innovation (ANII) for their funding, as well as the Universidad Católica del Uruguay (UCU) and the Universidad Iberoamericana, Ciudad de México, for their support and resources provided throughout this investigation.

REFERENCES

[1] Ltd. Aimagin Co. Waijung blockset for embedded system development, 2025. Online. Available: https://waijung1.aimagin.com/, [Accessed: Mar. 5, 2025].

[2] L. E. Anza, E. D. Ferreira, and H. E. Suárez. Design and construction of a prototype system for gait analysis for research in subjects with balance problems. In *2015 IEEE 6th Latin American Symposium on Circuits & Systems (LASCAS)*, pages 1–4, Montevideo, Uruguay, 2015.

[3] R. Barkataki, Z. Kalita, and S. Kirtania. Anthropomorphic design and control of a polycentric knee exoskeleton for improved lower limb assistance. *Intelligent Service Robotics*, 17:555–577, 2024.

[4] Marsi Bionics. Mak active knee, 2023. Online. Available: https://marsibionics.com/mak-active-knee/. [Accessed: Mar. 5, 2025].

[5] C. M. Bishop and H. Bishop. *Deep Learning Foundations and Concepts*. Springer Nature, 2024.

[6] M. Cardona, J. Yúdice, F. Huguet, G. López, C. Garcia Cena, and V. Solanki. Gait capture systems. In *SpringerBriefs in Applied Sciences and Technology*, pages 27–42. Springer, 1st edition, 2020.

[7] Z. Gao. Active disturbance rejection control: A paradigm shift in feedback control system design. In *Proceedings of the American Control Conference*, volume 5, pages 4989–4996, 2003.

[8] F. A. Gers, J. Schmidhuber, and F. Cummins. Learning to forget: Continual prediction with lstm. *Neural Computation*, 12(10):2451–2471, 2000.

[9] J. Han. From pid to active disturbance rejection control. *IEEE Transactions on Industrial Electronics*, 56(3):900–906, 2009.

[10] Hocoma. Lokomat, 2023. Online. Available: https://www.hocoma.com/us/solutions/lokomat/. [Accessed: Mar. 5, 2025].

[11] B. Kalita, J. Narayan, and S. K. Dwivedy. Development of active lower limb robotic-based orthosis and exoskeleton devices: A systematic review. *International Journal of Social Robotics*, 13:775–793, 2021.

[12] Vicon Motion Systems Ltd. Nexus: Software for motion capture in life sciences, 2025. Online. Available: https://www.vicon.com/software/nexus/, [Accessed: Mar. 5, 2025].

[13] MathWorks. Matlab: The language of technical computing, 2025. Online. Available: https://www.mathworks.com/products/matlab.html, [Accessed: Mar. 5, 2025].

[14] MathWorks. Simulink: Simulation and model-based design, 2025. Online. Available: https://es.mathworks.com/products/simulink.html, [Accessed: Mar. 5, 2025].

[15] Ottobock. C-brace: Knee orthosis, 2023. Online. Available: https://www.ottobock.com/es-ar. [Accessed: Mar. 5, 2025].

[16] M. Ramírez-Neria, G. Ochoa-Ortega, N. Lozada-Castillo, M. A. Trujano-Cabrera, J. P. Campos-López, and A. Luviano-Juárez. On the robust trajectory tracking task for flexible-joint robotic arm with unmodeled dynamics. *IEEE Access*, 4:7816–7827, 2016.

[17] J.-J. E. Slotine and W. Li. *Applied Nonlinear Control*. Prentice Hall, 1991.

[18] STMicroelectronics. Our technology starts with you, 2025. Online. Available: https://www.st.com/content/st_com/en.html, [Accessed: Mar. 5, 2025].

[19] Ltd. Suzhou Micro Actuator Technology Co. Myactuator: Integrated intelligent servo actuators for robotics, 2025. Online. Available: https://www.myactuator.com/, [Accessed: Mar. 5, 2025].

[20] V. I. Utkin, J. Guldner, and J. Shi. *Sliding Mode Control in Electromechanical Systems*. CRC Press, 2nd edition, 2017.

[21] R. Wilmart, E. Garone, and B. Innocenti. The use of robotics devices in knee rehabilitation: a critical review. *Muscle Ligaments and Tendons Journal*, 9:21, 2019.